Theoretical Description of Secondary Emission Reflecting Ultrafast Nonadiabatic Isomerization†

Susanne Hahn and Gerhard Stock*

Theoretical Quantum Dynamics, Faculty of Physics, University Freiburg, D-79104 Freiburg, Germany

Received: October 16, 2000; In Final Form: December 26, 2000

The fluorescence and resonance Raman emission of molecular systems undergoing ultrafast nonadiabatic isomerization is considered. Adopting a multidimensional model of vibronic coupling, explicit expressions for the continuous-wave spectra as well as for the time-resolved fluorescence spectrum are derived. To facilitate a simple eigenstate-free evaluation of the spectra of interest, various approximations are introduced. Employing a two-mode, two-state model of the photoisomerization of retinal, the validity of the approximations is studied numerically. The time-dependent eigenstate-free scheme is shown to provide an accurate approximation to the exact fluorescence spectrum. On the other hand, the well-known assumption that the emission stems from a vibrationally relaxed excited electronic state is not applicable in the case of ultrafast nonadiabatic isomerization processes under consideration.

I. Introduction

Photoinduced cis−trans isomerization in unsaturated hydrocarbons represents one of the best-studied reactions in organic photochemistry.[1−3] It is commonly believed that the twisting of a C═C double bond leads to a degeneracy of electronic states, thus resulting in a conical intersection of the corresponding potential energy surfaces (PESs). This phenomenon, sometimes referred to as "photochemical funnel," has been found to trigger ultrafast internal conversion processes, which lead to radiationless relaxation of the system from the electronic excited-state back to the ground state.[4−7] The quantum-mechanical description of photoinduced molecular dynamics on coupled PESs has been the subject of extensive theoretical investigations.[8−12] To account for the multidimensional nature of nonadiabatic photoisomerization processes, Domcke and co-workers have proposed a model Hamiltonian that includes the vibronic coupling of the lowest singlet states (S_0,S_1), a large-amplitude torsional mode, as well as one or two accepting modes for the radiationless transition.[13−14] Exact time-dependent wave packet calculations have been reported including up to four nuclear degrees of freedom, showing that the model is suitable to reveal basic features of photoisomerization and internal conversion dynamics. Alternatively, there have been first attempts to extend ab initio molecular dynamics simulations to describe electronic excited-state processes.[15−20] Very recently, this approach has also been employed to calculate electronic spectra.[21−23]

On the experimental side, numerous techniques of nonlinear optical spectroscopy have been employed to investigate ultrafast photophysical and photochemical processes.[24] Following resonant excitation by a continuous wave (cw) laser, one can monitor the secondary emission of the photoexcited molecule, which consists of coherent resonance Raman scattering as well as of incoherent fluorescence.[24−27] Both contributions reveal different aspects on the excited-state dynamics of the system:[28,29] The intensity of the resonance Raman fundamentals is a direct measure of the local gradient of the excited-state PES in the Franck−Condon region. The fluorescence emission, on the other hand, may yield valuable information on the electronic and vibrational relaxation dynamics of the system. Moreover, femtosecond time-resolved spectroscopy has been shown to yield a wealth of novel information on molecular photoreactions.[30−32] In particular, time-resolved fluorescence spectroscopy directly monitors the time evolution of the excited-state wave function.

In this work we are concerned with the theoretical description of fluorescence and resonance Raman spectroscopy of molecular systems undergoing ultrafast nonadiabatic isomerization. To this end we apply the standard theory of secondary emission[24−27] to the case of nonadiabatic photochemical reactions.[33] Employing the model system of ref 13, explicit expressions for the cw secondary-emission spectra as well as for the time-resolved fluorescence are derived. In particular, we discuss several approximations that allow us to utilize eigenstate-free wave packet propagation techniques to evaluate the signals of interest. The formulation is applied to a recently proposed two-state, two-mode model[39,40] of the photoisomerization of retinal in rhodopsin.[41,42] We present explicit simulations of cw absorption, resonance Raman and fluorescence spectra, as well as of the time-resolved fluorescence emission. The quality of the approximations introduced and the main effects of nonadiabatic isomerization are discussed in some detail.

II. Theory

A. Model System. To account for basic features of ultrafast nonadiabatic photoisomerization, Domcke and co-workers proposed a model that explicitly considers the vibronic coupling of the two lowest singlet states S_0,S_1.[13,14] Adopting a diabatic electronic representation with basis states $|\psi_0\rangle$, $|\psi_1\rangle$, the model Hamiltonian reads

$$H = \sum_{n=0,1} |\psi_n\rangle(T + V_n)\langle\psi_n| + (|\psi_0\rangle V_{01}\langle\psi_1| + \text{h.c.}), \qquad (2.1)$$

where T denotes the kinetic energy, and V_0,V_1 and V_{01},V_{10} are the diagonal and off-diagonal elements of the diabatic potential matrix, respectively.

† Part of the special issue "William H. Miller Festschrift".

* Address correspondence to: Gerhard Stock, Institute of Physical and Theoretical Chemistry, J. W. Goethe University, Marie-Curie-Str. 11, D-60439 Frankfurt, Germany.

10.1021/jp003788g CCC: $20.00
Published on Web 02/08/2001

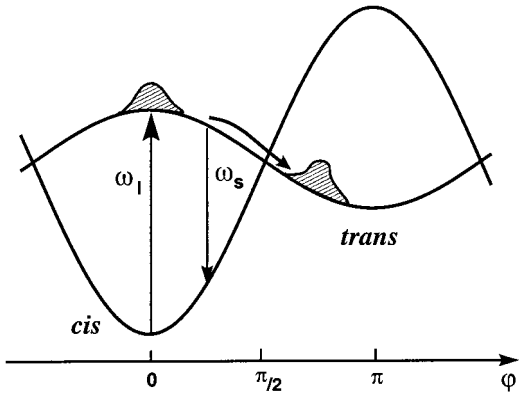

Figure 1. Adiabatic potential-energy surfaces of the two-state model of the cis−trans isomerization in rhodopsin. Shown is a cut of the potential-energy surfaces along the reaction coordinate n for $q = 0$. Upon vertical excitation by a laser of frequency ω_l, a vibrational wave packet is prepared that gives rise to spontaneous emission of frequency ω_s. Although the wave packet bifurcates at the conical intersections located at $\varphi = \pm(\pi/2)$, a fraction of it manages to climb back up to the S_1 cis conformation, thus causing recurrences of the time-resolved fluorescence emission.

The model comprises three types of vibrational modes: A reaction coordinate along which the molecule undergoes isomerization (the "isomerization mode" φ), a vibronically active mode that couples the two electronic states (the "coupling mode" q_c), and one or several totally symmetric modes that modulate the energy gap of the interacting states (the "tuning mode" q_t). The diabatic matrix elements of eq 2.1 are then given as

$$T = \frac{1}{2m}\frac{\partial^2}{\partial\varphi^2} + \sum_{j=t,c}\frac{\omega_j}{2}\frac{\partial^2}{\partial q_j^2} \tag{2.2}$$

$$V_n = V_n^R(\varphi) + \sum_{j=t,c} 1/2\omega_j\, q_j^2 + \delta_{1n}\kappa_j q_j \tag{2.3}$$

$$V_{01} = V_{10} = \lambda q_c \tag{2.4}$$

where m is the effective mass of the reaction coordinate, ω_j denotes the frequency of the jth vibrational mode, and κ_j represents its gradient of the excited-state PES with respect to the ground-state equilibrium geometry. The chemical aspects of the model are reflected by the torsional potentials

$$V_0^R(\varphi) = 1/2W_0(1 - \cos\varphi)$$
$$V_1^R(\varphi) = E_1 - 1/2W_1(1 - \cos\varphi) \tag{2.5}$$

which are drawn in Figure 1 for the model problem adopted below. Note that the excited-state potential $V_1^R(\varphi)$ is inverted, i.e., the upper diabatic electronic state for $n = 0$ (cis configuration) becomes the lower one for $\varphi = \pi$ (trans configuration). The corresponding adiabatic PESs of the model system exhibit a conical intersection, which has been shown to trigger irreversible isomerization and internal conversion dynamics on a femtosecond time scale.[9,13]

Figure 1 also serves to illustrate the photoexcitation and secondary emission of the system, which is described by the interaction Hamiltonian

$$H_{\text{int}}(t) = -\hat{\mu}E(t) \tag{2.6}$$

$$E(t) = E_l(t) + E_s(t) + \text{c.c.} \tag{2.7}$$

Here $\hat{\mu} = \hat{\mu}_{01} + \hat{\mu}_{10}$ represents the electronic transition dipole operator and $E_l(t) = \exp(-i\omega_1 t)$ and $E_l(t) = \exp(-i\omega_s t)$ denote the electric field of the cw excitation laser and the spontaneous emission, respectively. Assuming that the system is initially in its electronic and vibrational ground state, the laser prepares an excited-state wave packet that follows the slope of the PES from the cis to the trans configuration until it bifurcates at the conical intersection at $\varphi = \pi/2$. It is clear from Figure 1 that spontaneous emission can arise only during the time the wave packet is in the cis configuration, that is, the fluorescence directly monitors the time evolution of the excited-state wave function.

The model Hamiltonian (eq 2.1) is meant to account for the strongest interactions in the system that determine the photochemical reaction on the shortest time scales. The dynamics of these degrees of freedom is therefore treated exactly, while the effects of the remaining, presumably weaker, interactions and degrees of freedom may be taken into account in an approximate manner. At the simplest level of theory, one may introduce phenomenological decay rates in a density-matrix formulation. The Liouville-von Neumann equation for the total Hamiltonian can then be written as ($\hbar = 1$)

$$i\frac{\partial}{\partial t}\rho(t) = [H + H_{\text{int}}(t), \rho(t)] - i\Gamma(t) \tag{2.8}$$

where

$$\Gamma(t) = 1/T_1|\psi_1\rangle\rho_{11}(t)\langle\psi_1| + 1/T_2(|\psi_0\rangle\rho_{01}(t)\langle\psi_1| + \text{h.c.}), \tag{2.9}$$

and $\rho_{nm}(t) = \langle\psi_n|\rho(t)|\psi_m\rangle$. Equation 2.9 represents the standard Bloch damping matrix, which affects a decay of the excited-state population ρ_{11} with the rate $1/T_1$ as well as a decay of the coherences ρ_{01} and ρ_{10}, with the total dephasing rate $1/T_2 = 1/(2T_1) + 1/T^*$ in which $1/T^*$ is the pure dephasing rate.

It should be noted that the simple ansatz for the population relaxation in eq 2.9 represents an approximation in the case of a vibronically coupled system. This is because the damping matrix has been defined in the diabatic representation rather than in the adiabatic or eigenstate representation.[38] As explained above, however, spontaneous emission can occur only from the cis configuration and also not too close to the curve crossing (because of the ω_s^3 scaling of the spontaneous emission). In this region, the diabatic and adiabatic states coincide and the $1/T_1$ term in eq 2.9 indeed affects a population decay of the upper adiabatic state. Furthermore, it should be stressed that the molecular Hamiltonian (eq 2.1) in itself describes electronic and vibrational relaxation. The ansatz (eq 2.9) therefore is meant to provide a simple phenomenological description of the most essential relaxation effects that are not included in the microscopic treatment of the system.

B. Secondary Emission. To calculate the emission spectrum of the model system introduced above, the Liouville-von Neumann equation (2.8) is solved within time-dependent perturbation theory up to third order in $H_{\text{int}}(t)$, thus yielding the nonlinear electronic polarization $P^{(3)}(t) = \text{Tr}\{\hat{\mu}\rho^{(3)}(t)\}$. Within the rotating-wave approximation, we obtain[24,38]

$$P^{(3)}(t) = P^I(t) + P^{II}(t) \tag{2.10a}$$

$$P^I(t) = i^3\int_{-\infty}^{t} dt_3 \int_{-\infty}^{t_3} dt_2 \int_{-\infty}^{t_2} dt_1\, e^{-(t_3-t_2)/T_1}$$
$$e^{-(t-t_3+t_2-t_1)/T_2}\{E_s(t_3)E_l^*(t_1)E_l(t_2)R_1(t-t_3, t_3-t_2, t_2-t_1) +$$
$$E_s(t_3)E_l(t_1)E_l^*(t_2)R_2(t-t_3, t_3-t_2, t_2-t_1)\} \tag{2.10b}$$

$$P^{(\mathrm{II})}(t) = \mathrm{i}^3 \int_{-\infty}^{t} \mathrm{d}t_3 \int_{-\infty}^{t_3} \mathrm{d}t_2 \int_{-\infty}^{t_2} \mathrm{d}t_1 \, \mathrm{e}^{-(t-t_3+t_2-t_1)/T_2} E_s(t_2) E_l^*(t_1) E_l(t_3) R_3(t-t_3, t_3-t_2, t_2-t_1) \quad (2.10c)$$

where

$$R_1 = \mathrm{Tr}\,[\mathrm{e}^{\mathrm{i}H(t_2-t_1)}\,\hat{\mu}\mathrm{e}^{\mathrm{i}H(t_3-t_2)}\,\hat{\mu}\mathrm{e}^{\mathrm{i}H(t-t_3)}\hat{\mu}\mathrm{e}^{-\mathrm{i}H(t-t_1)}\hat{\mu}\rho^{(0)}] \quad (2.11a)$$

$$R_2 = \mathrm{Tr}\,[\hat{\mu}\mathrm{e}^{\mathrm{i}H(t_3-t_1)}\,\hat{\mu}\mathrm{e}^{\mathrm{i}H(t-t_3)}\,\hat{\mu}\mathrm{e}^{-\mathrm{i}H(t-t_2)}\hat{\mu}\mathrm{e}^{-\mathrm{i}H(t_2-t_1)}\rho^{(0)}] \quad (2.11b)$$

$$R_3 = \mathrm{Tr}\,[\hat{\mu}\mathrm{e}^{\mathrm{i}H(t_2-t_1)}\,\hat{\mu}\mathrm{e}^{\mathrm{i}H(t-t_2)}\,\hat{\mu}\mathrm{e}^{-\mathrm{i}H(t-t_3)}\hat{\mu}\mathrm{e}^{-\mathrm{i}H(t_3-t_1)}\rho^{(0)}] \quad (2.11c)$$

are three-time response functions accounting for the nonlinear response of the molecular system, and $\rho^{(0)}$ denotes the initial density operator of the system at time $t = -\infty$. Throughout this work we assume that the system is initially in its electronic and vibrational ground state $|\Psi_0\rangle$, i.e.,

$$\rho^{(0)} = |\Psi_0\rangle\langle\Psi_0| \quad (2.12)$$

The measured spectroscopic signal is proportional to the time average of the emission rate over an optical cycle

$$SE\sigma_{SE}(\omega_s,\omega_l) = \omega_l\omega_s^3\,\mathrm{Im}\,\langle E_s(t)\,P^{(3)}(t)\rangle \quad (2.13)$$

For interpretative purposes it is instructive to introduce the eigenstates $|\Psi_\alpha\rangle$ of the molecular Hamiltonian

$$H|\Psi_\alpha\rangle = \epsilon_\alpha|\Psi_\alpha\rangle \quad (2.14)$$

Inserting the eigenstate closure relation $\sum_\alpha|\Psi_\alpha\rangle\langle\Psi_\alpha| = 1$ into eq 2.11, the time integrations in eq 2.10 can be performed readily. We thus obtain the frequency-domain expression for the secondary-emission spectrum (eq 2.13), which consists of two parts.[24,38] The first contribution

$$\sigma_R(\omega_s,\omega_l) = \omega_l\omega_s^3 \sum_f |\sum_\alpha A_{f\alpha}(\omega_l)|^2\,\delta(\epsilon_0+\omega_l-\omega_s-\epsilon_f) \quad (2.15a)$$

$$A_{f\alpha}(\omega_l) = \frac{\langle\Psi_f|\hat{\mu}_{01}|\psi_\alpha\rangle\langle\Psi_\alpha|\hat{\mu}_{01}|\psi_0\rangle}{\epsilon_0+\omega_l-\epsilon_\alpha-\mathrm{i}/T_2} \quad (2.15b)$$

is recognized as the well-known KHD expression,[25] which describes the sharp Raman peaks that occur in the emission spectrum according to the conservation of energy. Hereby, ϵ_0 and ϵ_f denote the energy of the initial and final state, respectively. The second contribution can be written as

$$\sigma_F(\omega_s,\omega_l) = \frac{2\omega_l\omega_s^3}{T^*}\sum_{\alpha,\beta,f} A_{f\alpha}^*(\omega_l)A_{f\beta}(\omega_l)B_{\alpha\beta}[E_{f\alpha}^*(\omega_s)-E_{f\beta}(\omega_s)] \quad (2.16a)$$

$$B_{\alpha\beta} = (\epsilon_\alpha-\epsilon_\beta+\mathrm{i}/T_1)^{-1} \quad (2.16b)$$

$$E_{f\alpha}(\omega_s) = (\epsilon_f+\omega_s-\epsilon_\alpha+\mathrm{i}/T_2)^{-1} \quad (2.16c)$$

and accounts for the redistributed fluorescence that vanishes in the absence of pure dephasing ($1/T^* = 0$). Assuming that phenomenological lifetime broadening effects can be neglected ($1/T_1 = 0$), the latter expression simplifies to

$$\sigma_F(\omega_l,\omega_s) = \frac{4\omega_l\omega_s^3}{T_2T^*}\sum_{\alpha,f}|A_{f\alpha}(\omega_l)|^2\,|E_{f\alpha}(\omega_l)|^2 \quad (2.17)$$

Equations 2.10−2.13 and 2.15−2.16 are the standard expressions for the secondary emission in the time and energy domain, respectively.[24] From a practical point of view, the energy-domain expressions are convenient to treat systems having few levels. The time-domain expressions, on the other hand, are advantageous if the nonlinear response functions (eq 2.11) can be evaluated analytically, which is the case for the damped harmonic oscillator.

In the case of multidimensional vibronic-coupling problems, however, both formulations represent a serious computational problem. In the energy domain, eqs 2.15 and 2.16 can be evaluated as long as the Hamiltonian can be diagonalized. Employing standard methodology, nowadays this is feasible up to a dimension of $\approx 10^4$. In the time domain, on the other hand, one may transform eq 2.15 back into the time-dependent picture and obtain for the resonance Raman amplitude[26,43]

$$A_{f\leftarrow 0}(\omega_l) = \sum_\alpha A_{f\alpha}(\omega_l) = \int_0^\infty \mathrm{d}t\,\mathrm{e}^{\mathrm{i}\omega_l t}\,\mathrm{e}^{-t/T_2}\,C_f(t) \quad (2.18)$$

$$C_f(t) = \langle\Psi_f|\hat{\mu}_{01}\,\mathrm{e}^{-\mathrm{i}Ht}\,\hat{\mu}_{10}\mathrm{e}^{\mathrm{i}Ht}\,|\Psi_0\rangle \quad (2.19)$$

Note that eq 2.18 can be evaluated in terms of a *single* time-dependent propagation of the excited-state state vector. In the same way, the linear cw absorption spectrum is obtained as

$$\sigma_A(\omega_l) = 2\mathrm{Re}\;\omega_l\int_0^\infty \mathrm{d}t\,\mathrm{e}^{\mathrm{i}\omega_l t}\,\mathrm{e}^{-t/T_2}\,C_0(t) \quad (2.20)$$

Employing eqs 2.18 and 2.20, wave packet calculations of absorption and resonance Raman spectra have been reported up to a dimension of $\approx 10^7$.

Unfortunately, it is not that straightforward to calculate the fluorescence spectrum in the time-dependent formalism. This is because the evaluation of the three-time response functions (eq 2.11) makes it necessary to propagate the state vector *many times* back and forth in order to generate a three-dimensional time grid.[9,38] To facilitate a time-dependent wave packet evaluation of the fluorescence spectrum, we next consider the calculation of the time-resolved fluorescence following a short pump laser pulse. The analysis shows that the cw fluorescence spectrum can be described approximately by a pulsed excitation scheme and that the latter spectrum is readily evaluated by a wave packet calculation.

C. Time-Resolved Fluorescence. Employing fluorescence up-conversion techniques with femtosecond time resolution, it is also possible to measure the time evolution of the spontaneous emission. To describe this experiment, we assume that the electric field (eq 2.7) consists of a pump and a probe pulse

$$E_l(t) = \epsilon_l\,\mathrm{e}^{-\mathrm{i}\omega_l t}\mathrm{e}^{-t^2/(4g\tau_l^2)} \quad (2.21a)$$

$$E_s(t) = \epsilon_s\,\mathrm{e}^{-\mathrm{i}\omega_s(t-t_d)}\,\mathrm{e}^{-(t-t_d)^2/(4g\tau_s^2)} \quad (2.21b)$$

where τ_l and τ_n represent the pulse duration (FWHM) of the pump and probe field centered at time $t = 0$ and $t = t_d$, respectively. The amplitudes ϵ_l, ϵ_s are chosen to fulfill the normalization condition $\int \mathrm{d}t\,E_{l,s}(t) = 1$ and $1/g = 16\ln 2$. Disregarding all details of the up-conversion process, furthermore, we assume that the time-resolved fluorescence spectrum is equivalent to the dispersed stimulated-emission spectrum.[44] The latter is proportional to

$$I(\omega,t_d) = 2\mathrm{Im}\, E_s^*(\omega)P^{(3)}(\omega) \tag{2.22}$$

where $E_s(\omega)$ and $P^{(3)}(\omega)$ denote the Fourier transform of the probe field and the polarization, respectively. To calculate the time-resolved fluorescence, we therefore need to evaluate the nonlinear polarization (eq 2.10) with respect to the electric field (eq 2.21). Restricting ourselves to nonoverlapping pump and probe pulses, the second term in eq 2.10 vanishes, and the polarization $P^{(3)}(t)$ is given by $P^I(t)$.

It is instructive to rewrite the polarization in the following suggestive form[45,46]

$$P^{(3)}(t) = \int_{-\infty}^{t} \mathrm{d}t_d\, E_s(t_d)P^{\delta}(t,t_d) \tag{2.23}$$

$$P^{\delta}(t,t_d) = \mathrm{i}\int_{-\infty}^{t_d} \mathrm{d}t_2 \int_{-\infty}^{t_2} \mathrm{d}t_1\, \mathrm{e}^{-(t_d-t_2)/T_1} \mathrm{e}^{-(t-t_d+t_2-t_1)/T_2}[E_l^*(t_2)E_l(t_1)R_1(t-t_d, t_d-t_2, t_2-t_1) + E_l(t_2)E_l^*(t_1)R_2(t-t_d, t_d-t_2, t_2-t_1)] \tag{2.24}$$

where $P^{\delta}(t, t_d)$ can be interpreted as the third-order polarization for an arbitrary pump pulse and a δ-function probe pulse ($\tau_s = 0$). Combining eqs 2.22 and 2.24, we obtain for the corresponding impulsive stimulated-emission spectrum

$$I^{\delta}(\omega, t_d) = 2\mathrm{Im}\, \mathrm{e}^{-\mathrm{i}\omega t_d} P^{\delta}(\omega,t_d) = 2\mathrm{Im}\int_0^{\infty} \mathrm{d}t\, \mathrm{e}^{-\mathrm{i}\omega t} P^{\delta}(t+t_d, t_d) \tag{2.25}$$

The combination of eqs 2.23 and 2.24 thus suggests an advantageous evaluation scheme for pump−probe spectra:[47] One first calculates the impulsive spectrum $\propto I^{\delta}(t_d, \omega)$ and subsequently obtains via eq 2.23 the desired spectroscopic signals for probe pulses of arbitrary frequency and duration.

As has been discussed in detail elsewhere,[9,45,46] $I^{\delta}(t_d, \omega)$ represents an idealized time- and frequency-resolved emission spectrum, which is independent of laser-field properties and therefore directly reflects the time evolution of the excited-state wave function. Furthermore, the frequency-integrated impulsive signal $I^{\delta}(t_d) = \int d\omega I^{\delta}(t_d, \omega)$ is directly related to the time-dependent population probability of the optically excited electronic state.[9,46] Hence the time evolution of $I^{\delta}(t_d)$ directly monitors the nonadiabatic dynamics of the molecular system.

D. Approximate Calculation of Fluorescence Spectra. To make contact to the cw fluorescence spectrum (eq 2.16), let us now assume an experiment with a finite pump−pulse (2.21a) and a cw probe field $E_s(t) = \mathrm{e}^{-\mathrm{i}\omega_s t}$. In this case, the measured signal $\sigma_{F\tau}(\omega_s, \omega_l)$ is given by integrating eq 2.22 over all emission frequencies ω, thus yielding

$$\sigma_{F\tau}(\omega_s, \omega_l) = 2\mathrm{Im}\, \omega_l\omega_s^3 \int_0^{\infty} d\omega\, \delta(\omega-\omega_s) \int_{-\infty}^{0} \mathrm{d}t_d\, \mathrm{e}^{-\mathrm{i}\omega_s t_d} P^{\delta}(\omega,t_d) = \omega_l\omega_s^3 \int_0^{\infty} \mathrm{d}t_d\, I^{\delta}(\omega_s,t_d) \tag{2.26}$$

In accordance with physical intuition, eq 2.26 shows that the stationary fluorescence spectrum may be obtained from the impulsive time-resolved fluorescence spectrum through an integration over all emission times. Inserting again eigenstates, we obtain the corresponding frequency-domain expression

$$\sigma_{F\tau}(\omega_s,\omega_l) = \frac{4\omega_l\omega_s^3}{c_0} \sum_{\alpha,\beta,f} \mathrm{Re}\{\tilde{A}_{f\alpha}^*(\omega_l)\tilde{A}_{f\beta}(\omega_l)\} \mathrm{Re}\,\{\tilde{B}_{\alpha\beta}\, E_{f\beta}(\omega_s)\} \tag{2.27a}$$

$$\tilde{B}_{\alpha\beta} = \frac{\exp\{-\mathrm{i}g\tau_l^2\,(\epsilon_\beta - \epsilon_\alpha)/T_2\}}{\epsilon_\alpha - \epsilon_\beta + \mathrm{i}/T_1} \tag{2.27b}$$

$$\tilde{A}_{f\alpha}(\omega_l) = \frac{\langle\Psi_f|\hat{\mu}_{01}|\Psi_\alpha\rangle\langle\Psi_\alpha|\hat{\mu}_{10}|\Psi_0\rangle}{\exp\{g\tau_l^2\,(\epsilon_0+\omega_l-\epsilon_\alpha)(\epsilon_0+\omega_l-\epsilon_\alpha+2\mathrm{i}/T^*)\}} \tag{2.27c}$$

and $c_0 = \exp\{-4g\tau_l^2[(1/T^*)^2 - 1/(T^*T_2) + 1/(2T_2)^2]\}$. The expression of eq 2.27 for the fluorescence spectrum with pulsed excitation is seen to be quite similar to the corresponding expression of eq 2.16 for cw excitation. Essentially, the Lorentzian resonance factors $A_{f\alpha}$ and $B_{\alpha\beta}$ have been replaced by Gaussian resonance factors $\tilde{A}_{f\alpha}$ and $\tilde{B}_{\alpha\beta}$, thus reflecting the different excitation mechanism.

The analysis suggest that the time-domain expressions of eqs 2.25 and 2.26 may represent a suitable approximation to calculate the cw fluorescence spectrum. However, the practical evaluation of $P^{\delta}(t, t_d)$ is still cumbersome because of the entanglement of the time integrations over t_1 and t_2 in eq 2.24. Assuming that pure dephasing $1/T^*$ can be neglected during the pump−pulse, this entanglement can be resolved and the polarization $P^{\delta}(t, t_d)$ can be written as

$$P^{\delta}(t, t_d) = \mathrm{i}\, \mathrm{e}^{-(t-t_d)/T_2} \langle\Psi^{(1)}(t_d)|\hat{\mu}\mathrm{e}^{\mathrm{i}H(t-t_d)}\,\hat{\mu}\mathrm{e}^{-\mathrm{i}H(t-t_d)}|\Psi^{(1)}(t_d)\rangle \tag{2.28a}$$

$$|\Psi^{(1)}(t)\rangle = \mathrm{i}\int_{-\infty}^{t} \mathrm{d}t'\, \mathrm{e}^{-(t-t')/2T_1}\, E_l(t')\mathrm{e}^{-\mathrm{i}H(t-t')}\hat{\mu}\mathrm{e}^{-\mathrm{i}H\,t'}|\Psi_0\rangle \tag{2.28b}$$

Combining eqs 2.25, 2.26, and 2.28, we finally obtain

$$\sigma_{F\tau}(\omega_s,\omega_l) = 2\mathrm{Re}\, \omega_l\omega_s^3 \int_0^{\infty} \mathrm{d}t\, \mathrm{e}^{\mathrm{i}\omega_s t}\, \mathrm{e}^{-t/T_2}\, C_F(t) \tag{2.29a}$$

$$C_F(t) = \int_0^{\infty} \mathrm{d}t_d\, \langle\Psi^{(1)}(t_d)|\hat{\mu}\mathrm{e}^{\mathrm{i}H(t-t_d)}\,\hat{\mu}\mathrm{e}^{-\mathrm{i}\,H(t-t_d)}|\Psi^{(1)}(t_d)\rangle \tag{2.29b}$$

Equation 2.29 represents the desired eigenstate-free approximation of the fluorescence spectrum. Its evaluation requires three wave packet propagations, that is, the calculation of the wave function $|\Psi^{(1)}(t)\rangle$ prepared by the pump−pulse, the propagation of the excited-state wave packet $\mathrm{e}^{-\mathrm{i}H(t-t_d)}|\Psi^{(1)}(t_d)\rangle$, and the propagation of the ground-state wave packet $\langle\Psi^{(1)}(t_d)|\hat{\mu}_{10}\mathrm{e}^{\mathrm{i}H(t-t_d)}$.

To investigate the validity of eq 2.29, it is instructive to discuss various limiting cases of the excited-state wave function $|\Psi^{(1)}(t)\rangle$. First, we make contact to a popular approximation to calculate the cw fluorescence spectrum, that is, the assumption that the emission essentially stems from a vibrationally relaxed excited electronic state (see, e.g., ref 24). Here, the excited-state wave function is approximated by

$$|\Psi^{(1)}(t)\rangle = \mathrm{e}^{-t/2T_1}\, \mathrm{e}^{-\mathrm{i}\epsilon_1 t}\, |\Psi_1\rangle \tag{2.30}$$

where $|\Psi_1\rangle$ is the lowest eigenstate of the system on the upper PES. Insertion into eq 2.29b yields the simple expression[48]

$$C_F(t) \propto \langle\Psi_1|\hat{\mu}_{10}\mathrm{e}^{\mathrm{i}Ht}\,\hat{\mu}_{01}\,\mathrm{e}^{-\mathrm{i}Ht}|\Psi_1\rangle \tag{2.31}$$

As is shown in section IIIC, however, this approximation is not applicable to ultrafast nonadiabatic isomerization processes considered here. In this case, the fluorescence emission observed stems from a highly unrelaxed vibrational excited-sate manifold.

An approximation that accounts for the nonstationary nature of the initial state is obtained by assuming an impulsive (i.e., δ function) pump−pulse, thus yielding

$$|\Psi^{(1)}(t)\rangle = \mathrm{e}^{-\mathrm{i}(H-\mathrm{i}/2T_1)t}\,\hat{\mu}_{10}|\Psi_0\rangle \tag{2.32}$$

Within this approximation, the corresponding energy domain expression of eq 2.29 is again given by an expression quite similar to eq 2.16, except that the excitation amplitude changes to

$$A_{f\alpha}(\omega_l) = \frac{\langle\Psi_f|\hat{\mu}_{01}|\Psi_\alpha\rangle\langle\Psi_\alpha|\hat{\mu}_{10}|\Psi_0\rangle}{\epsilon_0 + \omega_l - \epsilon_\alpha - \mathrm{i}/T_2}$$
$$\langle\Psi_f|\hat{\mu}_{01}|\Psi_\alpha\rangle\langle\Psi_\alpha|\hat{\mu}_{10}|\Psi_0\rangle \tag{2.33}$$

that is, all eigenstates $|\Psi_\alpha\rangle$ are excited according to their Franck−Condon factors, irrespective of the excitation wavelength. It should be stressed that this limit can be achieved *either* by an ultrashort pump−pulse *or* in the case of strong electronic dephasing (independent of the duration of the excitation). It is noted that the numerical evaluation of the impulsive approximation [i.e., eqs 2.29 and 2.32] is much more involved than the evaluation of the popular approximation (eq 2.31). This is because the latter expression assumes a stationary initial state (eq 2.30), whereas the former takes into account the time evolution of the nonstationary initial state (eq 2.32).

III. Computational Results

A. Model and Numerical Details. As a representative model problem exhibiting nonadiabatic isomerization, we adopt a recently proposed electronic two-state model of the 11-cis → all-trans photoisomerization of retinal in rhodopsin.[39] It has been shown in ref 39 that this highly reduced quantum model with collective coordinates is able to qualitatively describe femtosecond pump−probe experiments on this system.[49−52] In particular, the onset of the photoproduct absorption band within 200 fs as well as the prominent 60 cm^{-1} beating of the time-resolved pump−probe signals could be explained in terms of multidimensional wave packet motion on nonadiabatically coupled PESs. In this work, we do not further discuss the photoreaction of rhodopsin but merely employ the model as a test problem to study the general effects of nonadiabatic photoisomerization on secondary-emission spectra.

Based on the isomerization Hamiltonian (eq 2.1) introduced above, the model comprises an effective reaction coordinate n and a collective vibronically active coordinate q, which describes the delocalized stretching motion of the polyene chain. Due to the low symmetry of retinal, this coordinate may simultaneously act as coupling and as tuning mode. The parameters of the model are (in eV): $m^{-1} = 4.84 \times 10^{-4}$, $E_1 = 2.48$, $W_0 = 3.6$, $W_1 = 1.09$, $\omega = 0.19$, $\kappa = 0.1$, $\lambda = 0.19$. General aspects of the model as well as the choice of parameters are discussed in refs 39 and 40.

The numerical methodology employed to solve Schrödinger's equation for multidimensional vibronically coupled systems has been discussed in detail in ref 9. In short, the state vector is expanded in a direct-product basis constructed from the two diabatic electronic states, 150 free-rotor states for the reaction coordinate, and 24 harmonic-oscillator states for the vibronically active coordinate. For the time-domain calculations, the resulting system of coupled first-order differential equations is integrated employing a standard Runge−Kutta−Merson algorithm. For the frequency domain calculations, the Hamilton matrix has been diagonalized using standard methods.

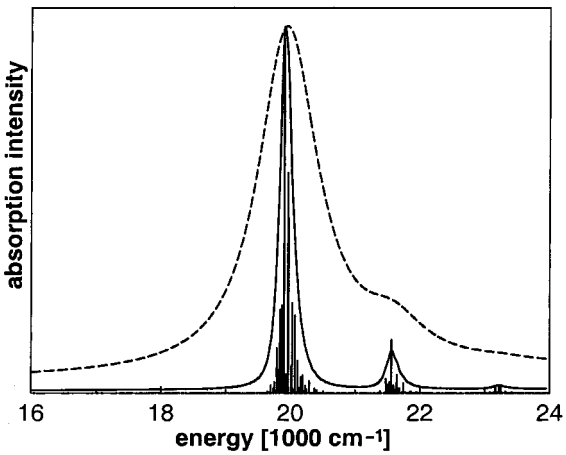

Figure 2. Cw absorption spectrum of the nonadiabatic isomerization model. Shown are the discrete stick spectrum of the bare two-mode model and the envelopes of the phenomenologically broadened spectra with $T_2 = 100$ fs (full line) and $T_2 = 10$ fs (dashed line).

B. Absorption and Resonance Raman Spectra. Let us first consider the cw absorption spectrum of the two-state, two-mode model introduced above. Employing eq 2.20, Figure 2 displays this spectrum for various phenomenological electronic dephasing rates $1/T_2$. The discrete stick spectrum of the bare two-mode model ($1/T_2 = 0$) is dense around the 0−0 transition at ≈20 000 cm^{-1} and exhibits a side maximum which results from the excitation of the vibronic mode q. While this peak is still well resolved for $T_2 = 100$ fs (full line), only a minor hump can be seen for $T_2 = 10$ fs (dashed line). The latter value approximately accounts for the width of the experimental absorption spectrum of rhodopsin.[41] In the following discussion, both values of T_2 will be used: $T_2 = 10$ fs as a realistic electronic dephasing time for a condensed-phase system, and $T_2 = 100$ fs as a stringent test of the approximate expressions derived above.

We continue with the discussion of the resonance Raman emission of the model. Employing eq 2.18 with $\omega_l = 20\,400$ cm^{-1}, Figure 3 shows this spectrum as obtained for the dephasing times (a) $T_2 = 100$ fs and (b) $T_2 = 10$ fs. The spectra exhibit the fundamental of the vibronically active mode q at ≈1470 cm^{-1} and excitations of the isomerization mode at multiples of ≈500 cm^{-1}. Note that the unperturbed vibrational frequency of the coupling mode is $\omega = 1532$ cm^{-1}. The strong vibronic interaction mediated by this mode thus leads to a significant decrease of its vibrational frequency in the electronic ground state. Furthermore, it is noted that due to the symmetry of the isomerization potentials (eq 2.5), only double excitations of the free-rotor levels are allowed. In harmonic approximation, the vibrational ground-state frequency of this mode is $\omega_R = \sqrt{W_0/2m} = 238$ cm^{-1}. The peaks at 474 and 947 cm^{-1} therefore correspond to $2\omega_R$ and $4\omega_R$, respectively. Relaxing the symmetry of the model potential (eq 2.5), one would also obtain the fundamental line of this mode. This coincides with the experimental resonance Raman spectrum of rhodopsin, which exhibits its most prominent low-frequency peak at ≈250 cm^{-1}.[53]

As resonance Raman scattering takes place during the electronic dephasing time T_2 (cf. eq 2.18), the relative intensities of the Raman excitations may depend crucially on the value of T_2. In the two-mode model under consideration, for example,

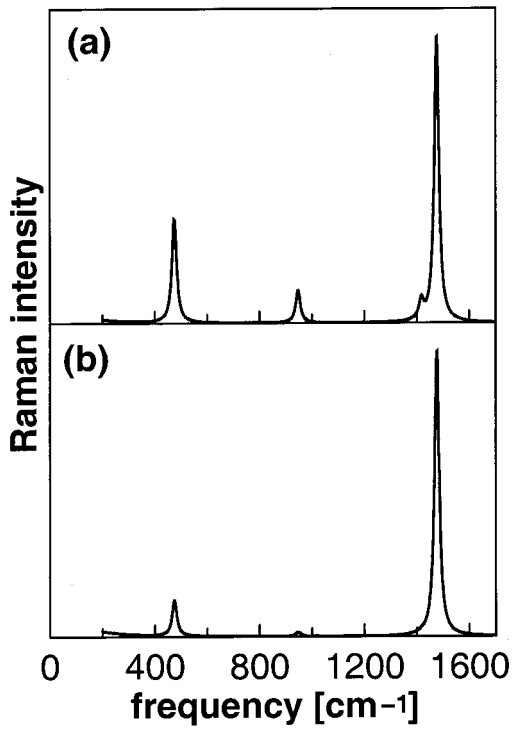

Figure 3. Resonance Raman spectrum of the two-mode isomerization model as obtained for the dephasing times (a) $T_2 = 100$ fs and (b) $T_2 = 10$ fs.

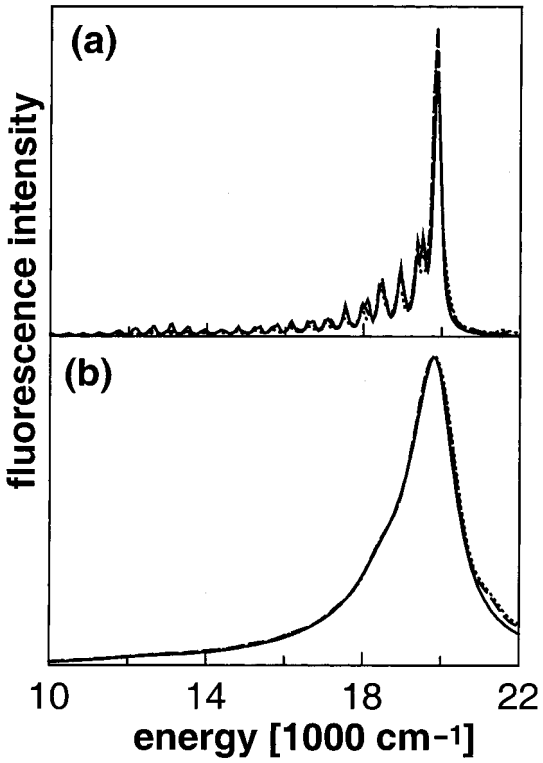

Figure 4. Cw fluorescence spectra of the isomerization model employing dephasing times (a) $T_2 = 100$ fs and (b) $T_2 = 10$ fs. Compared are results as obtained for the exact eigenstate calculations (full lines), the approximation with finite pump−pulse (dashed lines), and the impulsive approximation (dotted lines).

the relative excitation of the reaction mode is seen to differ significantly for $T_2 = 10$ and 100 fs. This is because the slope of the PES is flat along the reaction mode n but steep along the coupling mode q. The wave packet will therefore first follow the direction of the coupling mode before it reaches the slope of the reaction-mode potential. As a consequence, there is hardly a Raman excitation of the reaction mode for $T_2 = 10$ fs, which is in agreement with experiment.[53] Although the reaction coordinate clearly represents the most important nuclear degree of freedom of the isomerization model, the resonance Raman spectrum exhibits only minor excitation of this mode.

C. Fluorescence Emission. We turn to the discussion of the fluorescence emission of the two-mode isomerization model. Assuming resonant excitation ($\omega_l = 20\,000$ cm^{-1}), Figure 4 shows fluorescence spectra obtained for the dephasing times (a) $T_2 = 100$ fs and (b) T_2 10 fs. An excited-state lifetime of $T_1 = 300$ fs has been chosen to facilitate the convergence of the time integrations in eq 2.29. Because the cw spectra considered were found to be sensitive to the choice of T_1 only slightly, T_1 may be considered as purely technical parameter. Let us first discuss the exact results (full lines), which have been calculated via the eigenstate expressions (eq 2.16). The spectrum exhibits a prominent maximum at ≈20 000 cm^{-1}, which corresponds to resonance fluorescence out of the Franck−Condon region. The maximum is followed by emission that extends to the far-infrared, thus reflecting the decreasing electronic energy gap along the isomerization coordinate (cf. Figure 1). It is noted that far-infrared emission has been reported for various cis−trans photoisomerization systems, including rhodopsin,[54] bacteriorhodopsin,[55] and all-trans retinal.[56] While for $T_2 = 10$ fs the fluorescence spectrum is essentially structureless, for $T_2 = 100$ fs the spectrum exhibits a progression of peaks corresponding to free rotor levels of the reaction coordinate with a level spacing of $2\omega_R$. We note in passing that there also is a weak maximum around 13 000 cm^{-1}, which is due to two competing effects that occur when the wave packet moves down the slope of the reaction coordinate: On one hand, we find a decrease of the overlap integrals when the wave packet moves away from the Franck−Condon region; on the other hand, there is an increase of the number of vibrational levels in the electronic ground state that become accessible via a vertical spontaneous emission process.

Being integrated over all emission times (cf. eq 2.26), the cw fluorescence spectra merely yield time-averaged information. To obtain a more detailed picture of the fluorescence emission and the associated excited-state dynamics, it is therefore instructive to consider the time-resolved fluorescence spectrum. Hereby, we restrict ourselves to the discussion of the impulsive emission spectrum defined in eq 2.25. As discussed above, this idealized time- and frequency-resolved signal is independent of laser-field properties and therefore reflects directly the excited-state dynamics of the system. Figure 5 shows the impulsive emission spectrum as obtained for the two-mode isomerization model with $1/T_1 = 0$ and $T_2 = 10$ fs. The signal exhibits an ultrafast initial decay within 200 fs, which is followed by prominent recurrences of the emission with a period of ≈500 fs. As has been discussed in detail in ref 39, these recurrences reflect coherent wave packet motion along the reaction-mode potential $V_1^R(\varphi)$. As illustrated in Figure 1, the photoinduced wave packet thereby undergoes quasiperiodic motion on coupled adiabatic PESs. It has been suggested that this nonadiabatic wave packet motion gives rise to the 60 cm^{-1} beating observed in femtosecond transient transmittance experiments.[50] Comparing Figures 4 and 5, it is clear that the time-resolved fluorescence spectrum provides much more information on the nonadiabatic photochemical reaction than does the cw fluorescence spectrum.

Next we wish to study the performance of the approximations introduced in section IID. In particular, we consider the time-

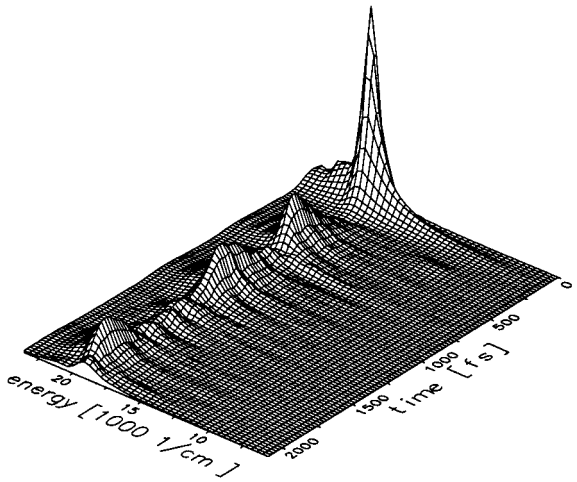

Figure 5. Impulsive time- and frequency resolved fluorescence spectra of the two-mode isomerization model. The prominent recurrences of the emission reflect quasiperiodic wave packet motion on coupled adiabatic potential-energy surfaces.

dependent expression (eq 2.29), which approximates the fluorescence spectrum following cw excitation by the corresponding spectrum following pulsed excitation. As the duration of the pump pulse essentially affects a broadening of the excitation spectrum (cf. eq 2.27), the pulse durations have been chosen to coincide with the total dephasing time, i.e., (a) $\tau_1 = T_2 = 100$ fs and (b) $\tau_1 = T_2 = 10$ fs, respectively. Furthermore, we have considered the limiting case of impulsive excitation, that is, a δ-function pump−pulse (cf. eq 2.32). Figure 4 compares the results as obtained for the exact eigenstate calculations (full lines), the approximation with finite pump−pulse (dashed lines), and the impulsive approximation (dotted lines). The data are seen to be in good overall agreement, even in the case of $T_2 =$ 100 fs, which exhibits numerous spectral details. While this result may be expected for resonant excitation, it is interesting to study the validity of the approximation (eq 2.29) for near-resonant excitation. Detuning the excitation frequency ω_l, the fluorescence spectrum of the isomerization model exhibits a frequency shift, which is qualitatively reproduced by the approximation (data not shown). The finding of a Stokes shift of the fluorescence due to a change of the excitation frequencies indicates that the emissions stem from an unrelaxed excited-state vibrational manifold.

The result obtained already suggests the inadequacy of the alternative approximation mentioned above, that is, the assumption that the fluorescence emission essentially stems from the lowest eigenstate of the system on the upper PES (cf. eq 2.30). For example, it is not clear what eigenstate is the lowest eigenstate on the upper PES, because the eigenstates of the vibronically coupled system (eq 2.1) are given as linear combinations of both diabatic electronic states $|\psi_0\rangle$, $|\psi_1\rangle$. Somewhat ambiguously, we have chosen the "lowest eigenstate $|\Psi_1\rangle$ with dominant $|\psi_1\rangle$ character", that is, $\in_1 = 2.453$ eV and $|\langle\Psi_1|\psi_1\rangle| = 0.87$. Assuming furthermore resonant excitation and $T_2 = 100$ fs, Figure 6(a) compares the exact calculation of the fluorescence spectrum (full line) to the results obtained from the approximate expression (eq 2.31) employing the eigenstate $|\Psi_1\rangle$ (dotted line). Obviously, the approximation largely disagrees with the reference calculation. Somewhat better results are obtained when the eigenstate corresponding to the main resonant peak of the absorption spectrum is used (dashed line). The situation is also different under low-resolution conditions, i.e., if a dephasing time of $T_2 = 10$ fs is employed. Although the underlying assumptions are not justified, the approximation

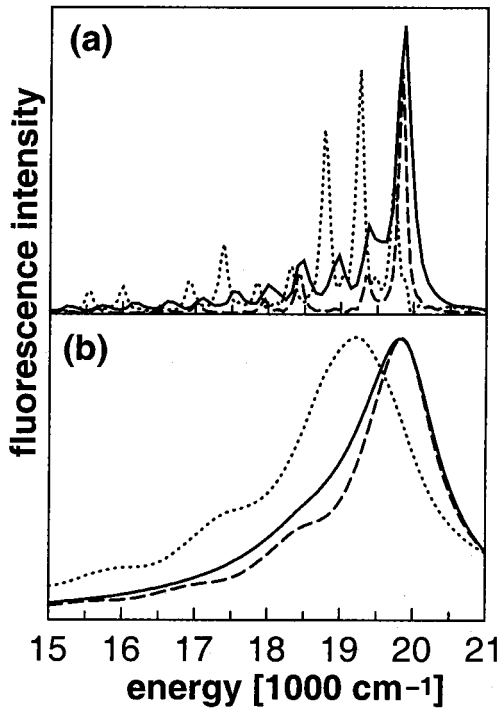

Figure 6. Cw fluorescence spectra of the isomerization model for (a) $T_2 = 100$ fs and (b) $T_2 = 10$ fs. Compared are exact results (full line) and the relaxed-state approximation (dotted and dashed lines).

is found to qualitatively reproduce the low-resolution fluorescence spectrum shown in Figure 6b. This finding may explain the surprising success of this ansatz in modeling the fluorescence spectrum in the case of ultrafast photodynamics.[21,22]

IV. Conclusions

We have given a microscopic description of fluorescence and resonance Raman spectroscopy of molecular systems undergoing ultrafast nonadiabatic isomerization. Adopting a multidimensional model of vibronic coupling, explicit expressions for the cw secondary emission spectra as well as for the time-resolved fluorescence spectrum have been derived. It has been shown that the stationary fluorescence spectrum may be obtained from the impulsive time-resolved fluorescence spectrum through an integration over all emission times. Various approximations have been discussed that allow us to employ eigenstate-free wave packet propagation techniques, thus facilitating the treatment of large molecular systems. To investigate the validity of these approximations, we have performed detailed numerical studies employing a recently proposed two-mode, two-state model of rhodopsin. Hereby, the approximate eigenstate-free scheme has been found to provide an accurate approximation to the exact fluorescence spectrum, even in the case of relatively high frequency resolution. On the other hand, the popular assumption that the emission stems from a vibrationally relaxed excited electronic state has been proven invalid in the case of the ultrafast nonadiabatic isomerization processes under consideration.

We have studied to what extent ultrafast nonadiabatic isomerization processes are reflected in the secondary emission of the molecular system. The information obtained by cw absorption and resonance Raman experiments is limited by ultrafast electronic dephasing processes. In the condensed phase, the total electronic dephasing time is typically in the order of 10 fs. Since isomerization as well as electronic and vibrational relaxation has hardly yet started, cw absorption and resonance

Raman spectra of systems with ultrafast electronic dephasing may yield only limited information on these processes. This is demonstrated, for example, by the finding that the Raman intensity of the reaction mode is rather weak, although this coordinate clearly represents the most important nuclear degree of freedom of the model.

The fluorescence spectrum, on the other hand, in principle monitors the photoreaction during the entire excited-state lifetime. Hereby, the Stokes shift of the emission reflects the variation of the electronic energy gap during the photoreaction, whereas the fluorescence quantum yield allows us to estimate the excited-state lifetime of the molecular system. Moreover, the measurement of the dynamical evolution of the fluorescence emission may provide a wealth of additional information on the photochemical reaction. It has been shown that the time- and frequency-resolved fluorescence spectrum directly monitors the time evolution of the excited-state wave function, thereby providing a real-time measurement of the nonadiabatic photoreaction. In the case of the rhodopsin model, for example, the recurrences of time-resolved spectrum clearly reveal the motion of the vibrational wave packet along the reaction coordinate.

Acknowledgment. We thank Wolfgang Domcke for stimulating and helpful discussions. This work has been supported by the Deutsche Forschungsgemeinschaft and the Fonds der Chemischen Industrie.

References and Notes

(1) Michl, J.; Bonačić-Koutecký, V. *Electronic Aspects of Organic Photochemistry*; Wiley: New York, 1990.
(2) Klessinger, M.; Michl, J. *Excited States and Photochemistry of Organic Molecules*; VCH: New York, 1995.
(3) Orlandi, G.; Zerbetto, F.; Zgierski, M. *Chem. Rev.* **1991**, *91*, 867.
(4) Bernardi, F.; Olivucci, M.; Robb, M. A. *Chem. Soc. Rev.* **1996**, *25*, 321.
(5) Garavelli, M.; Bernardi, F.; Olivucci, M.; Vreven, T.; Klein, S.; Celani, P.; Robb, M. A. *Faraday Discuss.* **1998**, *110*, 51.
(6) Woywod, C.; Livingood, W. C.; Frederick, J. F. *J. Chem. Phys.* **2000**, *112*, 613.
(7) Hofmann, A.; R. de Vivie-Riedle. *J. Chem. Phys.* **2000**, *112*, 5054.
(8) Köppel, H.; Domcke, W.; Cederbaum, L. S. *Adv. Chem. Phys.* **1984**, *57*, 59.
(9) Domcke, W.; Stock, G. *Adv. Chem. Phys.* **1997**, *100*, 1.
(10) Schneider, R.; Domcke, W.; Köppel, H. *J. Chem. Phys.* **1990**, *92*, 1045.
(11) Manthe, U.; Köppel, H. *J. Chem. Phys.* **1990**, *93*, 345.
(12) Schinke, R. *Photodissociation Dynamics*; University Press: Cambridge, 1993.
(13) Seidner, L.; Domcke, W. *Chem. Phys.* **1994**, *186*, 27.
(14) Seidner, L.; Stock, G.; Domcke, W. *J. Chem. Phys.* **1995**, *103*, 3998.
(15) Vreven, T.; Bernardi, F.; Garavelli, M.; Olivucci, M.; Robb, M. A.; Schlegel, H. B. *J. Am. Chem. Soc.* **1997**, *119*, 12687.
(16) Berweger, C. D.; Müller-Plathe, F.; van Gunsteren, W. F. *J. Chem. Phys.* **1998**, *108*, 8773.
(17) Frank, I.; Hutter, J.; Marx, D.; Parinello, M. *J. Chem. Phys.* **1998**, *108*, 4060.
(18) Ben-Nun, M.; Martínez, T. J. *Chem. Phys. Lett.* **1998**, *298*, 57.
(19) Bittner, E. R.; Kosov, D. S. *J. Chem. Phys.* **1999**, *110*, 6645.
(20) Tsiper, E. V.; Chernyak, V.; Tretiak, S.; Mukamel, S. *J. Chem. Phys.* **1999**, *110*, 8328.
(21) Mercer, I. P.; Gould, I. R.; Klug, D. R. *J. Phys. Chem. B* **1999**, *103*, 7720.
(22) Cárdenas, A. E.; Krems, R.; Coalson, R. D. *J. Phys. Chem. A* **1999**, *103*, 9469.
(23) Ben-Nun, M.; Martínez, T. J. *J. Phys. Chem. A* **1999**, *103*, 10517.
(24) Mukamel, S. *Principles of Nonlinear Optical Spectroscopy*; University Press: Oxford, 1995.
(25) Kramers, H. A.; Heisenberg W. *Z. Phys.* **1925**, *31*, 681. Dirac, P. A. M. *Proc. R. Soc. London* **1927**, *114*, 710.
(26) Lee, S.-Y.; Heller, E. J. *J. Chem. Phys.* **1979**, *71*, 4777.
(27) Original work on secondary emission includes Huber, D. L. *Phys. Rev.* **1967**, *158*; **1968**, *170*, 418; **1969**, *178*, 93; *Phys. Rev. B* **1970**, *1*, 3409. Hizhnyakov, V.; Tehver, I. *Phys. Status Solidi* **1967**, *21*, 755. Shen, Y. R. *Phys. Rev. B* **1974**, *9*.
(28) Mathies, R. A.; Smith, S. O.; Palings, I.; Wiley: New York, 1987; Vol. 2.
(29) Myers-Kelley, A. *J. Phys. Chem. A* **1999**, *103*, 6891.
(30) Zewail, A. H. *Femtochemistry−Ultrafast Dynamics of the Chemical Bond;* World Scientific: Singapore, 1994.
(31) Manz, J., Wöste, L., Eds. *Femtosecond Chemistry;* VCH: New York, 1995.
(32) Elsaesser, T., Fujimoto, J. G., Wirsma, D. A., Zinth, W., Eds. *Ultrafast Phenomena XI*; Springer: Heidelberg, 1998.
(33) Vibronic-coupling effects in resonance Raman spectra have been discussed by many authors. See, e.g., refs 34−36. Fluorescence emission from coupled electronic states has been considered in refs 37 and 38.
(34) Henneker, W. H.; Siebrand, W.; Zgierski, M. Z. *Chem. Phys. Lett.* **1976**, *43*, 11; *J. Chem. Phys.* **1981**, *74*, 6560.
(35) Coalson, R. D.; Kinsey, J. L. *J. Chem. Phys.* **1986**, *85*, 4322.
(36) Reber, C.; Zink, J. I. *J. Chem. Phys.* **1992**, *96*, 2681. Bitner, T. W.; Zink, J. I. *J. Am. Chem. Soc.* **2000**, *122*, 10631.
(37) Meyer, H.-D.; Köppel, H. *J. Chem. Phys.* **1984**, *81*, 2605.
(38) Stock, G.; Domcke, W. *J. Chem. Phys.* **1990**, *93*, 5496.
(39) Hahn, S.; Stock, G. *J. Phys. Chem. B* **2000**, *104*, 1146.
(40) Hahn, S.; Stock, G. *Chem. Phys.* **2000**, *259*, 297.
(41) Birge, R. R. *Biochim. Biophys. Acta* **1990**, *1016*, 293.
(42) Ottolenghi, M.; Sheves, M. *Isr. J. Chem.* **1995**, *35*.
(43) Heller, E. J. *Acc. Chem. Res.* **1981**, *14*, 368.
(44) Effects of the detection scheme (e.g., finite time and frequency resolution) are readily accounted for by convolution of the impulsive emission spectrum with the detector response function.[9]
(45) Pollard, W.; Mathies, R. A. *Annu. Rev. Phys* **1992**, *43*, 497.
(46) Stock, G.; Domcke, W. *Phys. Rev. A* **1992**, *45*, 3032.
(47) Hahn, S.; Stock, G. *Chem. Phys. Lett.* **1998**, *296*, 137.
(48) Allowing for finite temperature, eq 2.31 is replaced by Tr $\{|\hat{\mu}_{10}\, e^{iHt}\, \hat{\mu}_{01}\, e^{-iHt}\rho_1\}$, where ρ_1 denotes the thermal density matrix with respect to the excited electronic state.
(49) Peteanu, L. A.; Schoenlein, R. W.; Mathies, R. A.; Shank, C. V. *Proc. Natl. Acad. Sci. U.S.A.* **1993**, *90*, 11762.
(50) Wang, Q.; Schoenlein, R. W.; Peteanu, L. A.; Mathies, R. A.; Shank, C. V. *Science* **1994**, *266*, 422.
(51) Chosrowjan, H.; Mataga, N.; Shibata, Y.; Tachibanaki, S.; Kandori, H.; Shichida, Y.; Okada, T.; Kouyama, T. *J. Am. Chem. Soc.* **1998**, *120*, 9706.
(52) Haran, G.; Morlino, E. A.; Matthes, J.; Callender, R. H.; Hochstrasser, R. M. *J. Phys. Chem. A* **1999**, *103*, 2202.
(53) Loppnow, G. L.; Mathies, R. A. *Biophys. J.* **1988**, *54*, 35.
(54) Koechendoerfer, G. G.; Mathies, R. A. *J. Phys. Chem.* **1996**, *100*, 14526.
(55) Dobler, J.; Zinth, W.; Kaiser, W.; Oesterhelt, D. *Chem. Phys. Lett.* **1988**, *144*, 215.
(56) Takeuchi, S.; Tahara, T. *J. Phys. Chem. A* **1997**, *101*, 3052.